ORIGINAL ARTICLE

OIT3 mediates macrophage polarization and facilitates hepatocellular carcinoma progression

Shuai Yang[1,2] · Jiangang Zhang[1] · Yanquan Xu[1] · Jingchun Wang[1] · Huakan Zhao[3,4] · Juan Lei[3,4] · Yu Zhou[3,4] · Yu Chen[3,4] · Lei Wu[3,4] · Mingyue Zhou[3,4] · Lu Zheng[5] · Xiaohui Ji[3,4] · Yongsheng Li[1,3,4]

Abstract

Hepatocellular carcinoma (HCC) is one of the most common causes of cancer-related mortality; however, effective immunotherapy strategies are limited because of the immunosuppressive tumor microenvironment. Macrophages are essential components of the HCC microenvironment and are related to poor prognosis. Here, we evaluated the attributes of paracancer tissues in tumor immunity and progression using public databases. Based on the abundance of immune cells estimated by CIBERSORT, we performed weighted gene co-expression network analysis and found a specific module associated with M2 macrophages. Through analyzing interaction networks using Cytoscape and public datasets, we identified oncoprotein-induced transcript 3 (OIT3) as a novel marker of M2 macrophages. Overexpression of *OIT3* remodeled immune features and reprogrammed the metabolism of M2 macrophages. Moreover, compared with wildtype macrophages, *OIT3*-overexpressing macrophages further enhanced the migration and invasion of co-cultured cancer cells. Additionally, *OIT3*-overexpressing macrophages promoted tumorigenesis and cancer development in vivo. Taken together, the findings demonstrate that OIT3 is a novel biomarker of alternatively activated macrophages and facilitates HCC metastasis.

Keywords Hepatocellular carcinoma · OIT3 · Alternatively activated macrophages · Weighted gene co-expression network analysis · Paracancer · Migration and invasion

Shuai Yang and Jiangang Zhang have contributed equally to this work.

✉ Lu Zheng
  xqyyzl1@163.com

✉ Xiaohui Ji
  15023245186@163.com

✉ Yongsheng Li
  lys@cqu.edu.cn

1   Clinical Medicine Research Center, Xinqiao Hospital, Army Medical University, Chongqing 400037, China

2   Department of Pathology, the 958th Hospital, Southwest Hospital, Army Medical University, Chongqing 400038, China

3   Department of Medical Oncology, Chongqing University Cancer Hospital, Chongqing 400030, China

4   Chongqing Key Laboratory for Tumor Metastasis and the Translational Research of Individualized Diagnosis and Treatment, Chongqing University Cancer Hospital, Chongqing 400030, China

5   Department of Hepatobiliary Surgery, Xinqiao Hospital, Army Medical University, Chongqing 400037, China

Abbreviations

AMPK	Adenosine 5-monophosphate-activated protein kinase
BMDM	Bone marrow-derived macrophage
DEG	Differentially expressed gene
GEO	Gene expression omnibus
HCC	Hepatocellular carcinoma
ICIs	Immune checkpoint inhibitors
mTOR	The mechanistic target of rapamycin
OIT3	Oncoprotein-induced transcript 3
TAM	Tumor-associated macrophage
TME	The tumor microenvironment
WGCNA	Weighted gene co-expression network analysis

Introduction

Hepatocellular carcinoma (HCC) is a prevalent form of liver cancer that is characterized by rapid disease progression with high postsurgical recurrence and high metastatic rate [1, 2]. Recent developments in immune checkpoint inhibitors (ICIs), including nivolumab and

pembrolizumab, improved survival and provided additional options to treat HCC, but the objective response rates of these promising treatments remained < 20% [2–6]. Thus, further investigation of the roles of tumor-associated immune cells is important for exploring reasonable therapeutic strategies and reducing HCC mortality.

Histological normalcy, in general, implies normal biology. Thus, histologically normal tissues dissected adjacent to cancer (paracancer tissues) are used as healthy controls for cancer studies to reduce individual-specific and anatomical site-specific effects. However, paracancer tissues are significantly different from healthy normal tissues. Recent studies have suggested that paracancer tissues are in a pre-neoplastic state comprising morphologically normal but molecularly altered cells, and abnormally infiltrated immune cells [7–10]. Macrophages are essential for maintaining tissue homeostasis, especially for regulating the tumor microenvironment (TME) [11]. According to their polarization states, macrophages are usually classified as classically activated (M1) and alternatively activated (M2). Studies on human tumor samples have demonstrated that the proportion of macrophages (tumor-associated macrophages, TAMs) plays a crucial role in tumor progression, metastasis, and recurrence after treatment that usually display an M2-like phenotype [12–14]. Therefore, a better understanding of the interaction of anticancer therapies with M2 macrophages may pave the way for novel HCC immunotherapy.

In this study, we focused on the infiltrated immune cells in paracancer tissues considering that these immune cells may play pivotal roles in tumor immunosuppression, progression, and metastasis. Taken together, we aimed to explore new potential immunotherapeutic targets for HCC metastasis.

Materials and methods

Human and mouse samples

Human HCC and paracancer samples were provided by the Department of Pathology of the 958th Hospital (Chongqing, China). Eight-week-old male C57BL/6 mice were purchased from the Animal Institute of the Academy of Medical Science (Beijing, China). Eight-week-old BALB/c nude mice were purchased from Vital River Laboratory Animal Technology Co., Ltd. (Beijing, China). All mice were maintained under specific pathogen-free conditions, and experiments were conducted in accordance with the relevant guidelines approved by the Institutional Animal Care and Use Committee of the Army Medical University.

Cell culture and treatments

The femur and tibia samples were obtained from 8-week-old C57BL/6 mice, severed proximal to each joint, and flushed with cold RPMI medium (Gibco) to collect bone marrow cells using a syringe. The bone marrow cells were cultured in RPMI-1640 containing 10% (v/v) FBS (Gibco) and 20 ng/mL of mouse GM-CSF (catalog no. 315–03, PeproTech) for 7 days to obtain bone marrow-derived macrophages (BMDMs). The iBMDM cell line was a gift from Prof. Feng Shao, Ph.D. (National Institute of Biological Sciences, Beijing, China). The iBMDM cells were cultured in DMEM (Gibco) supplemented with 10% (v/v) FBS (Gibco). To generate M1 and M2 macrophages, BMDMs or iBMDMs were stimulated with LPS (100 ng/mL; catalog no. L4524, Sigma-Aldrich) + IFN-γ (20 ng/mL; catalog no.315–05; PeproTech), or IL-4 (10 ng/mL, catalog no. 214–14; PeproTech) *plus* IL-13 (10 ng/mL, catalog no.210–13; PeproTech) for 12–24 h, respectively.

For transfection, iBMDM cells were washed twice with PBS and then incubated in DMEM (10% FBS) with lentivirus GFP vectors of Mock or LV-Oit3 (20 μL, 1×10^8 TU/ml; Genechem) mixed with transfection reagent (40 μL, $25 \times$; Genechem) for 48 h and selected with puromycin (2.5 μg/mL) for 20 days, according to the manufacturer's instructions.

H22 cells were purchased from the Type Culture Collection of the Chinese Academy of Sciences and cultured in RPMI-1640 containing 10% FBS. In the co-culture assay, iBMDMs (5×10^5 cells/well) were seeded in a 6-well plate, and H22 cells (5×10^5 cells/well) were added to the culture supernatants. After co-culturing for 24–48 h, H22 cells were collected from the supernatants by centrifugation at 1000 rpm at 4 °C for 5 min.

Hepa1-6 cells were purchased from the Type Culture Collection of the Chinese Academy of Sciences and cultured in DMEM containing 12% FBS. In the migration assays, iBMDMs (2.5×10^5 cells/well) were seeded in a 24-well plate in complete medium. Hepa1-6 cells, pre-starved for 6 h, were seeded onto the filters of the top chambers (5×10^4 cells/chamber) with 0.8-μm polycarbonate membrane (catalog no.3422, Corning) in serum-free medium. Next, Hepa1-6 cells (2.5×10^5 cells/well) were seeded in the 24-well plate, with only complete medium in the control group. The cells were co-cultured for 8–12 h before fixing with paraformaldehyde for 30 min. Invasion assays were performed as described in a previous study [15]. Briefly, the filters were covered with 50 μL of matrigel (diluted to 200–300 μg/mL; catalog no.356234, Corning) and incubated for 6 h at 37 °C. Furthermore, the cells were seeded for migration assays and co-cultured for 24 h before fixation. Next, the fixed filters were stained

with 0.2% crystal violet after removing the non-invading cells that remained on the upper surface of the filters. Cells were visualized using a phase-contrast microscope. The ratios were calculated as the gray value of cells versus the area of the microscopic field using ImageJ (https://cnij.imjoy.io/).

Data source and identification of differentially expressed genes (DEGs)

The array datasets of GSE45436, GSE62232, GSE112790, and GSE121248 were downloaded from the Gene Expression Omnibus (GEO) database (http://www.ncbi.nlm.nih.gov/geo/). After removing specimens whose clinical information failed to match with their sample names, 426 tumor specimens and 97 normal specimens were selected. We extracted and normalized the expression data using the *mas.5* function in the affy R package (version 1.64.0). Probes of the normalized data were converted to gene symbols according to the GPL570 annotation information platform. Probes without matched genes were eliminated, and the average value was calculated for genes corresponding to more than one probe. Further, batch effects were removed from the normalized data using the *ComBat* function in the sva *R* package (version 3.34.0). Based on the normalized expression data, DEGs were identified using the limma R package (version 3.42.3) and filtered with an adjusted p value < 0.01, $|\log_2 FC| > 1$, and average gene expression > 0.01 *ACTB*.

Estimated immune scores

The stromal/immune score was calculated using the ESTIMATE R package (version 1.0.13) that estimated the presence of infiltrating stromal/immune cells in the TME. The paracancer samples were processed using the ESTIMATE algorithm on default settings; and three scores were generated: stromal, immune, and estimate scores representing fractions of stromal cells, abundances of infiltrated immune cells, and combined immune and stromal score, respectively.

Estimated fractions of immune cells in CIBERSORT

CIBERSORT, a versatile computational method, is frequently used to estimate the abundance of immune cell types from bulk tissue transcriptomes. The expression data without $\log_2$ transformation were uploaded to the CIBERSORT website (https://cibersort.stanford.edu/) and computed in relative and absolute models together with the signature gene files of LM22 and 1000 permutations. The fractions of the 22 immune cell types were downloaded for further analyses.

Weighted gene co-expression network analysis

Weighted gene co-expression network analysis (WGCNA) was performed using R package as described previously [16, 17]. First, paracancer samples were filtered through a clustering dendrogram based on their Euclidean distance. With a cutoff value of height at 60, two samples were excluded. Further, the proper soft thresholding power was selected in *pickSoftThreshold* function according to the approximate scale-free topology (*R* square of 0.85) and mean connectivity criteria. Next, co-expression modules were constructed on the default (unsigned) setting, with softPower of 4, minModuleSize of 30, and mergeCutHeight value of 0.25. Additionally, we associated the expression modules with an abundance of infiltrated immune cells (*R* codes could be found in the supplement materials). Finally, the corresponding gene module was extracted, and the node and edge files (top 200, ranked in weight values) were imported into Cytoscape.

Interaction analysis in cytoscape

The WGCNA edge and node files of the red module were imported into Cytoscape (version 3.6.1), the sizes and colors of circles were mapped to the degrees of nodes, and the border and color of lines were applied to map the values of weights in Edges. The interaction network was visualized in the attribute circle layout.

Real-time quantitative PCR

Total RNA was extracted using RNAiso Plus (Cat No.9109, Takara, Otsu, Shiga, Japan) according to the manufacturer's instructions and was reverse transcribed into cDNA using PrimeScript RT reagent Kit with gDNA Eraser (Takara). The mRNA expression was assessed by real-time quantitative polymerase chain reaction (RT-qPCR) using TB Green® Premix Ex Taq™ II (Takara) on BioRad CFX96 (Bio-Rad, CA). Relative gene expression was calculated using the $2^{-\Delta\Delta Ct}$ method and normalized to expression of *Hprt* mRNA. The primers used in this experiment are listed in Supplementary Table 1.

Western blotting

Cells were lysed in radioimmunoprecipitation assay (RIPA) lysis buffer with phenylmethylsulfonyl fluoride for 30 min on ice and centrifuged at 12,000 rpm at 4 °C for 15 min before the supernatant was collected. Cell lysates were quantified using bicinchoninic acid assay (catalog no. P0068; Beyotime, Jiangsu, China). Western blotting analysis was performed as described previously [18]. Briefly, after sodium dodecyl sulfate (SDS)–polyacrylamide gel electrophoresis and blocking, membranes were incubated with primary

antibodies at 4 °C overnight. The primary antibodies used were against OIT3 (catalog no. ab139190; Abcam), CD163 (catalog no. ab182422, Abcam), NOS2 (catalog no. 18985–1-AP, Proteintech), ARG1 (catalog no. 16001–1-AP, Proteintech), AMPKa (catalog no. AF1627, Beyotime), mTOR (catalog no. 2983, Cell Signaling Technology), Snail (catalog no. 3879, Cell Signaling Technology), vimentin (catalog no. 5741, Cell Signaling Technology), and β-actin (catalog no. 3700, Cell Signaling Technology). After five washes with tris-buffered saline/Tween 20, the membranes were incubated at 20 °C for 60 min with horseradish peroxidase-conjugated goat anti-rabbit antibody (catalog no. A0208, Beyotime) and goat anti-mouse antibody (catalog no. A0216, Beyotime), respectively. The protein bands were visualized using an enhanced chemiluminescence plus Western blotting detection kit (catalog no. 1705061, Bio-Rad). The relative expression levels of the protein bands were calculated using ImageJ (https://cnij.imjoy.io/).

Immunohistochemistry

Immunohistochemistry (IHC) of tumor sections was performed as previously described[19]. The slides were stained with primary CD3 antibody (MAB-0740, MXB) or CD45 antibody (Kit-0024, MXB) and imaged under a light microscope (BX63, Olympus Microsystems).

Nude mouse tumorigenicity assay

Eighteen 5-week-old nude mice were randomly divided into three groups. In the negative control group, serum-free PBS (100 μL) containing H22 cells (1×10^6) was subcutaneously injected into the right flank of the mice. For the treatment groups, serum-free PBS (100 μL) containing H22 cells (1×10^6) and Mock-iBMDM (1×10^6) or LV-Oit3-iBMDM (1×10^6) was injected into the corresponding site of mice. The tumor volume was calculated as: (length $\times$ Width^2)/2.

Statistical analysis

Statistical analyses were performed in ggplot2 (version 3.3.5) and ggspubr (version 0.4.0) R packages using R software (version 3.6.3) described in previous methods [20]. All the biological experiment data were processed in GraphPad Prism 8 (GraphPad Software, Inc.), expressed as the mean ± SD, and were analyzed using either one-way ANOVA or two-tailed unpaired Student's t-test. For each parameter of all data presented, * indicates $p < 0.05$, ** indicates $p < 0.01$, *** indicates $p < 0.001$, and **** indicates $p < 0.0001$.

Results

Infiltrated immune cells converge in paracancer tissues

After analyzing GEO microarray datasets (GSE45436, GSE62232, GSE112790, and GSE121248) based on the GPL570 annotation platform, we found 1,186 DEGs that were upregulated in paracancer tissues. The top DEGs in paracancer tissues, such as *CLEC4M*, *CXCL14*, *CLEC4G*, and *CLEC1B*, were identified (Fig. 1a). Of interest, these genes were reported to be involved in the inflammatory immune response process [21–24]. Based on the GO annotation, we identified three biological process terms related to immune and inflammatory responses (Fig. 1b). Consistent with results of previous studies [8, 9], the immune and stromal scores were higher in the paracancer tissues than those in cancer tissues according to the ESTIMATE algorithm (Fig. 1c). The immune cell markers, such as CD163 (macrophages), CD3 (T cells), CD45 (leukocytes), and CD19 (B cells), were significantly upregulated in paracancer tissues than in cancer tissues (Fig. 1d). We further assessed CD45 and CD3 in HCC samples and observed that the positively stained regions were frequently located in the paracancer tissues. Taken together, these results confirm enrichment of immunological characteristics in paracancer tissues.

Construction of gene networks and identification of modules in paracancer tissues

The WGCNA is frequently used to identify co-expressed networks and co-expression modules [25, 26]. We imported the expression matrix of 1186 DEGs upregulated in the paracancer tissues to WGCNA to determine co-expression genes with similar traits. Hierarchical clustering of paracancer samples was performed to exclude two outliers with a height cutoff of 60 (Fig. 2a); 95 samples were included in the subsequent analysis. The adequate soft threshold power was 4, by setting an R square of 0.85, according to the trade-off between scale-free topology and mean connectivity (Fig. 2b). We identified modules using average linkage hierarchical clustering and a dynamic tree cut. The red and black modules were independent and were not embedded in any other modules (Fig. 2c). The brown module was inserted in blue and turquoise modules (Fig. 2c) that were significantly similar to each other according to the hierarchical clustering of module eigen genes and heatmap plot of the adjacent entities in the eigen genes (Fig. 2d). Taken together, red and black modules were identified as rational co-expression modules for further analysis.
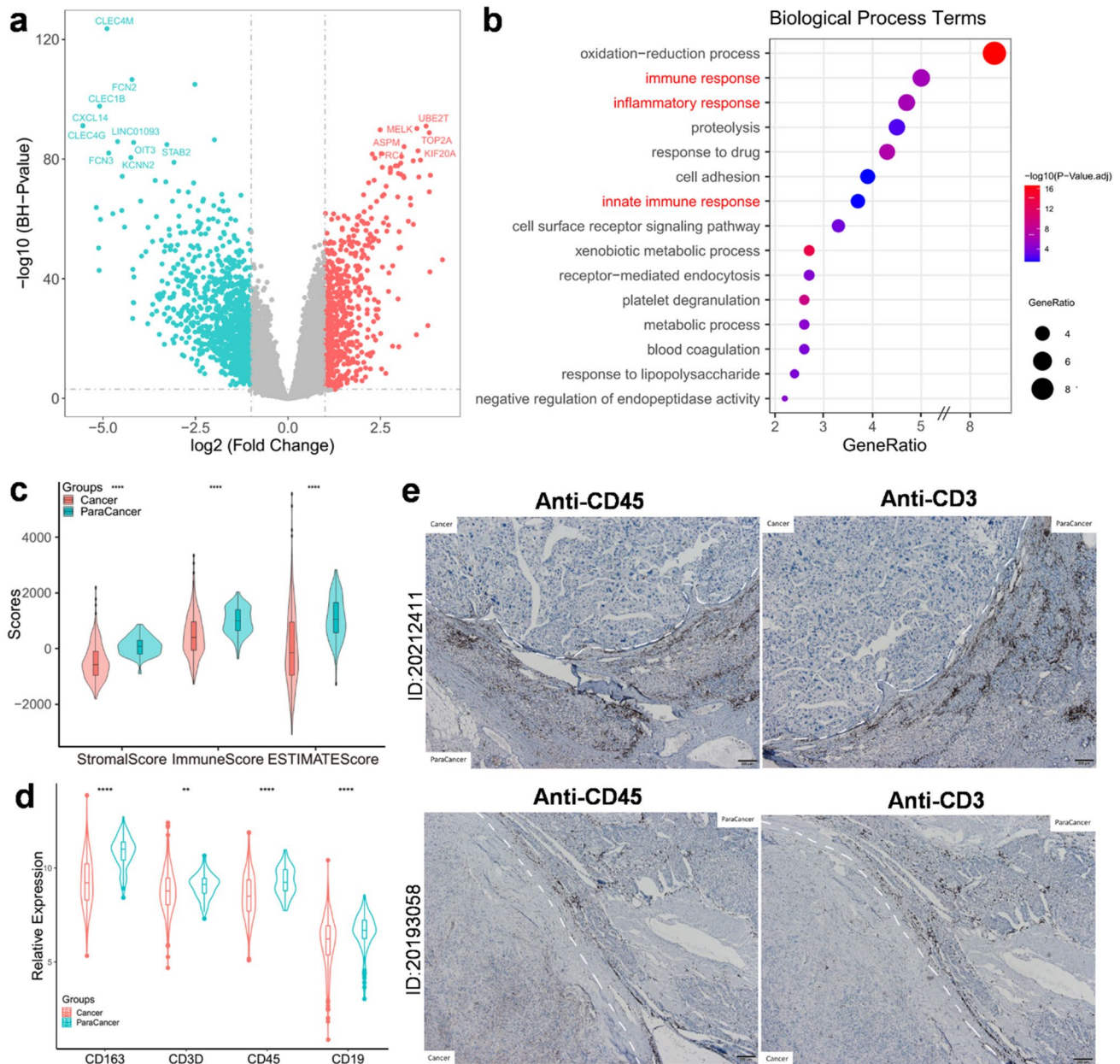
Fig. 1 Immune cells converged in paracancer versus cancer tissues. **a** Volcano plots of DEGs in GEO array dataset, top DEGs ($-\log_{10}$(BH p-value) > 80, |$\log_2$FC| > 2.5) were labeled. Red dots represented upregulated genes in cancer tissues, while green dots represented upregulated genes in paracancer tissues. **b** Bubble plots of top 15 biological process terms of GO annotation which were ordered by gene ratio of enriched process ($p < 0.01$). **c** Stomal scores and immune scores (inferred by ESTIMATE) in paracancer and cancer tissues plotted by violin box plots ($p < 0.001$). **d** Expression of CD163, CD3, CD45, and CD19 in paracancer versus cancer tissues ($p < 0.01$). **e** Immunohistochemistry of CD45 and CD3 in paracancer and cancer tissues from two independent HCC patients

Association of specific module with composition of infiltrated immune cells in paracancer tissues

To better characterize the immunological characteristics of these modules, we estimated the abundance of infiltrated immune cell types in paracancer samples using CIBERSORT based on a deconvolution approach [27–29]. By calculating correlation between the modules and immune cell fractions, we found that the red module was more relevant to the M2 macrophages ($r = 0.62$, $p < 0.001$) than black module (Fig. 3a). For each module, WGCNA define a quantitative measure of module membership (MM) as the correlation of the module eigen gene and the gene expression profile. To refine the analysis, we constructed a scatterplot of gene significance (GS) for M2 macrophage *versus* MM in the red module. Here, GS and MM were highly
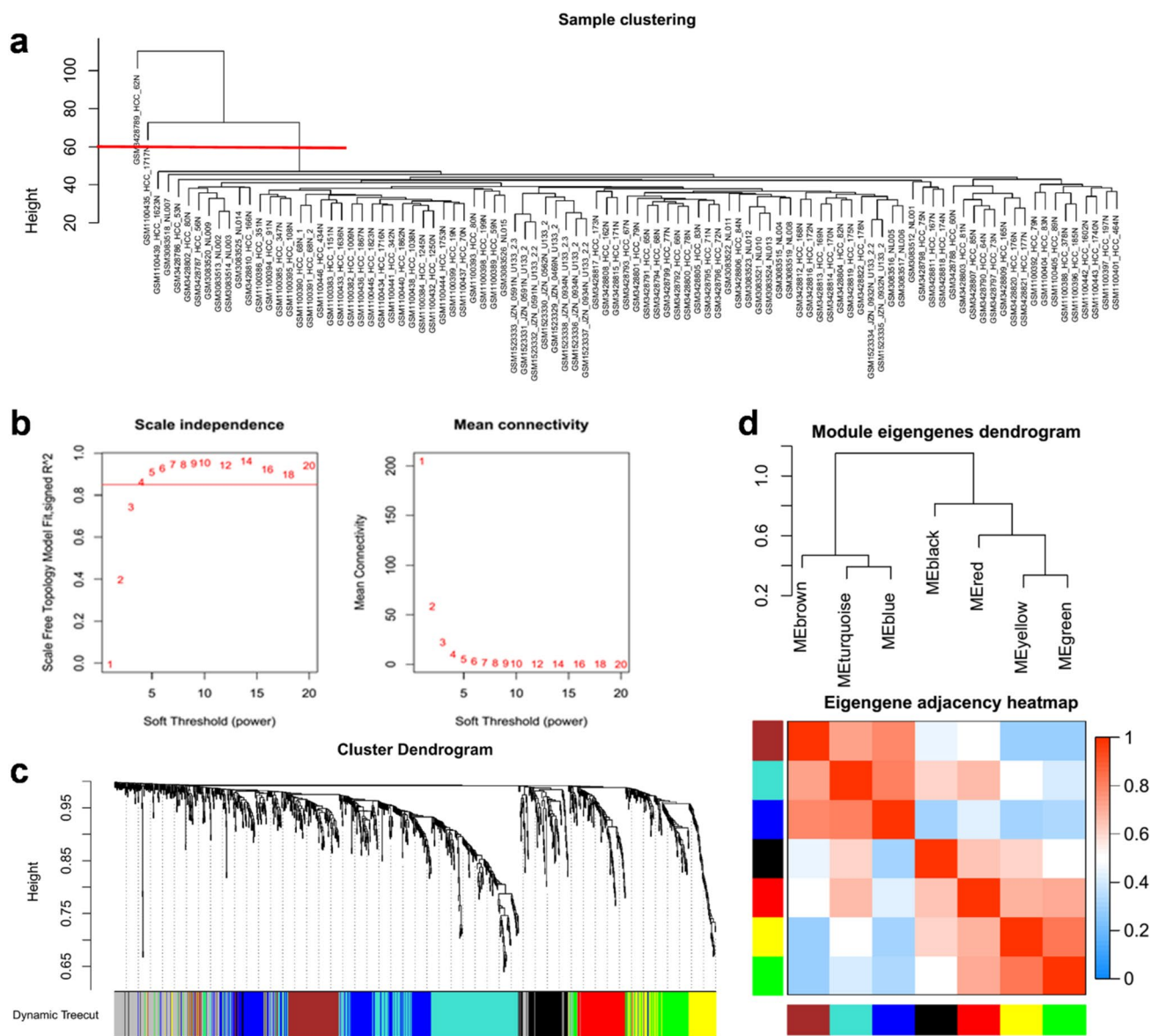
Fig. 2 Construction of weighted gene co-expression network with the upregulated genes in paracancer. **a** Exclusion of outlier samples through clustering dendrogram. Two samples were excluded by setting cutoff value of height to 60 from total of 97 paracancer samples. **b** Determination of soft threshold power on a trade-off between scale free topology (left panel, R square $= 0.85$) and mean connectivity (right panel). **c** Identified modules by average linkage hierarchical clustering and dynamic tree cut. Red and Black modules were high consistency and independent without inserted by other modules. **d** Hierarchical clustering of module eigengenes (up panel) and heatmap plot of the adjacencies in the eigengene network (down panel)

correlated ($r = 0.79$, $p < 0.001$) (Fig. 3b), illustrating that the genes significantly associated with M2 macrophages were also the most important (central) elements of the red module associated with M2 macrophages. To further target and screen meaningful hub genes, we imported WGCNA edge and node files into Cytoscape. The candidate genes of the red module were ranked according to the degrees of nodes and weights of edges (Fig. 3c). Moreover, a

majority of the genes have been reported as biomarkers of M2 macrophages, such as *MS4A6A*, *CD163*, *CLEC4G*, *VSIG4*, *MARCO*, *LYVE1*, and *MRC1* [30–35]. Based on the correlation analysis, the expression of *OIT3* was found to significantly correlate with the abundance of M2 macrophages, with maximum correlation coefficient between candidate genes (Fig. 4). Therefore, we inferred that OIT3 may be a novel marker of M2 macrophages.
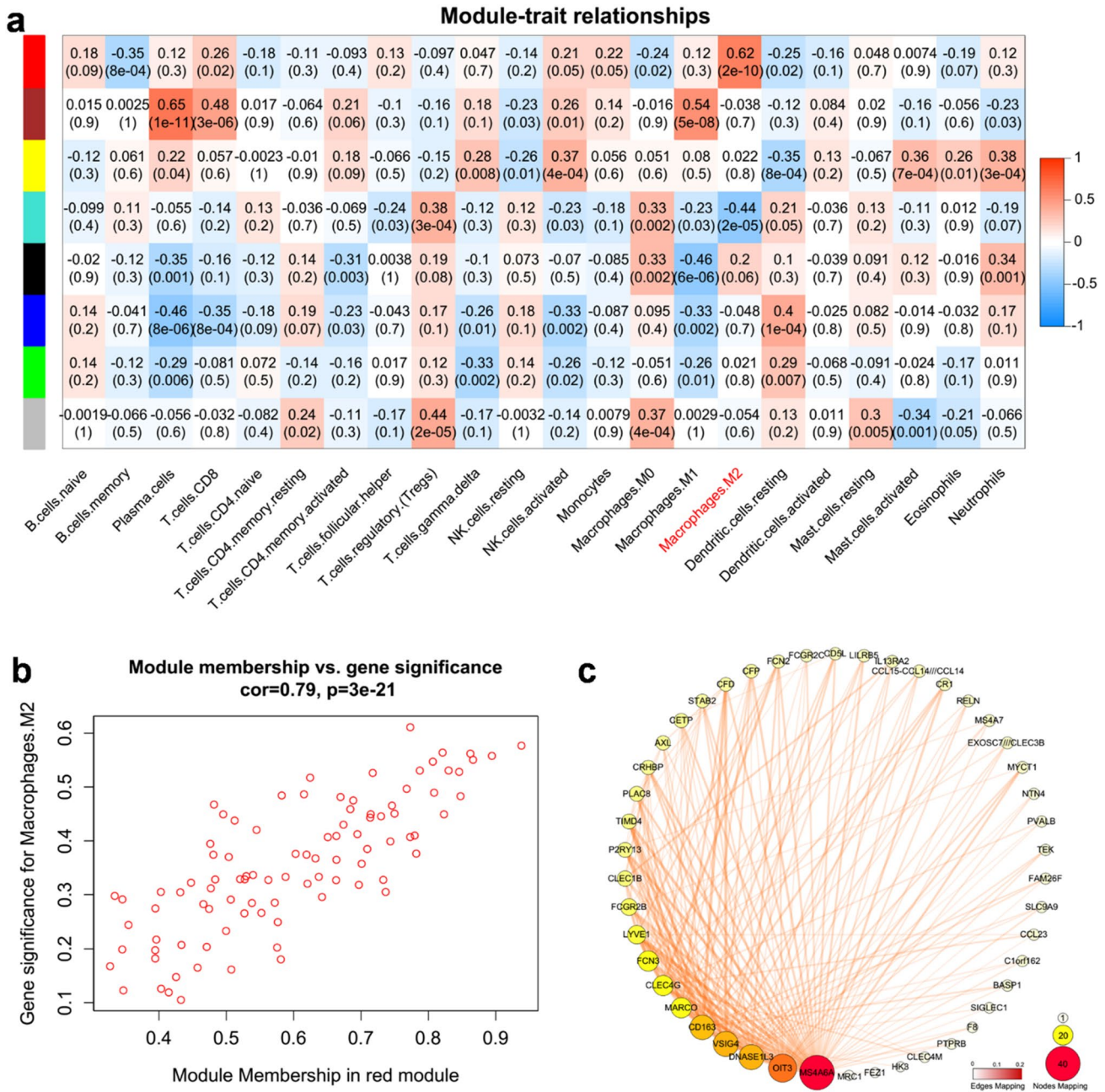
Fig. 3 Identification of modules associated with the fraction of infiltrated immune cells in paracancer tissues. **a** Heatmap of the correlation between module eigengenes and fractions of infiltrated immune cells calculated by CIBERSORT. Red module represents a high correlation with M2 macrophages. **b** A scatterplot of gene significance for M2 macrophages *versus* module membership in the red module. The significant correlation implied the eigengenes in red module tend to be highly correlated with M2 macrophages. **c** WGCNA edge and node files were imported into Cytoscape (top 200 edges ranked by weight values). The size and color of circles mapped to the values of degree of Nodes, and the border and color of lines mapped to the values of weights in Edges

OIT3 is a novel biomarker of M2 macrophages

To validate the inference, we searched related data from the GEO dataset. Consistent with expression of *ARG1* and *MRC1*, the expression of *OIT3* was significantly higher in M2 macrophages than that in M0 and M1 macrophages in both the array dataset (GSE80185, Fig. 5a) and RNA-seq dataset (GSE158094, Fig. 5b). Moreover, in vitro experiments with BMDM and iBMDM cell lines indicated that OIT3 was highly expressed in M2 macrophages at the gene and protein levels than in M0 and M1 macrophages (Fig. 5c–f).
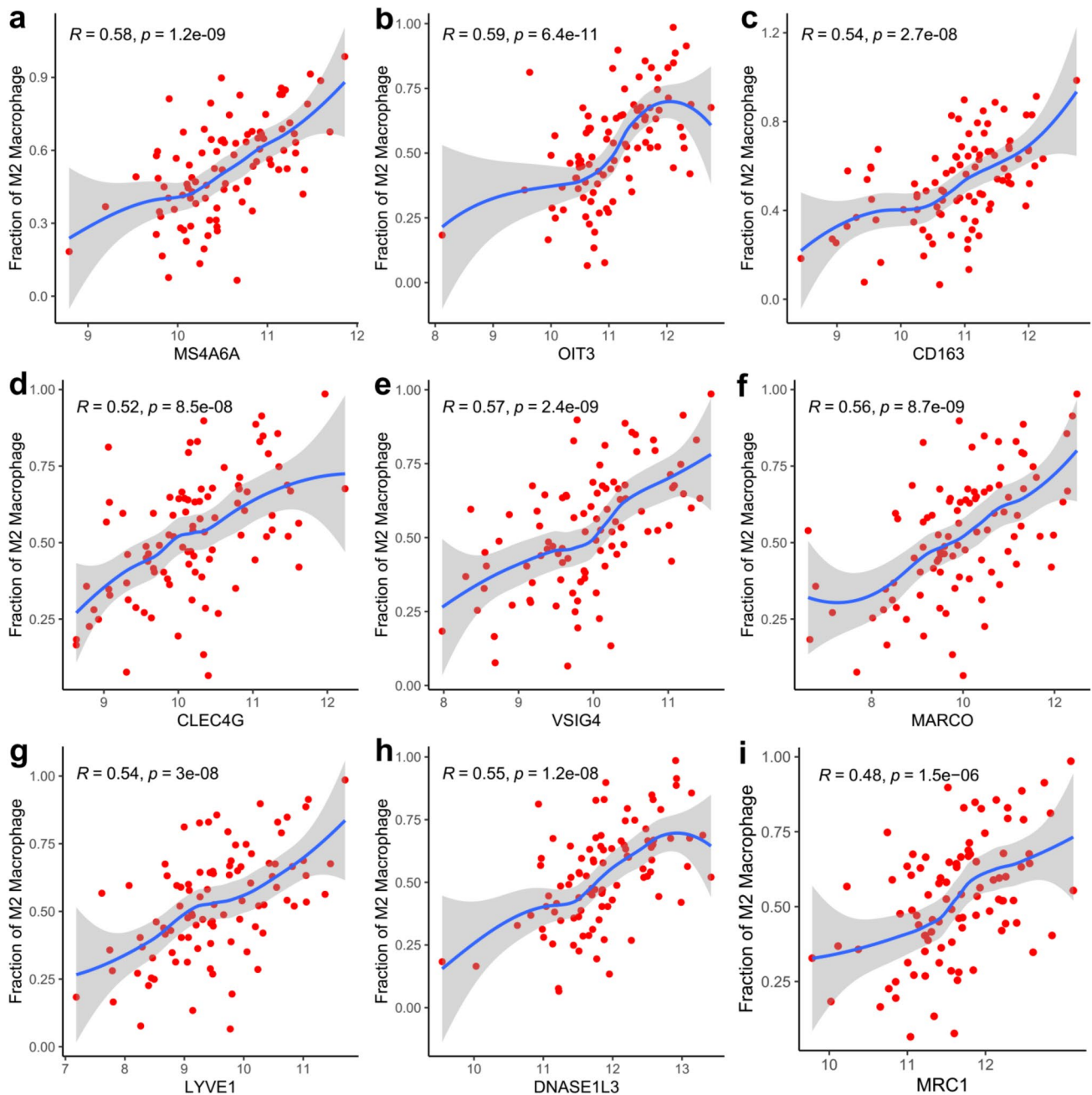
Fig. 4 Correlation analysis of the expression of candidate biomarkers with the fractions of M2 macrophage. Spearman correlation analysis was performed in the abundance of M2 and the expression of MS4A6A ($R = 0.58$, $p < 0.001$, **a**), OIT3 ($R = 0.59$, $p < 0.001$, **b**), CD163 ($R = 0.54$, $p < 0.001$, **c**), CLEC4G ($R = 0.52$, $p < 0.001$, **d**), VSIG4 ($R = 0.57$, $p < 0.001$, **e**), MARCO ($R = 0.56$, $p < 0.001$, **f**), LYVE1 ($R = 0.54$, $p < 0.001$, **g**), DNASE1L3 ($R = 0.55$, $p < 0.001$, **h**) and MRC1 ($R = 0.48$, $p < 0.001$, **i**)

Overexpression of *OIT3* reprograms immunity and metabolism of M2 macrophages

The overexpression lentiviral vector of *OIT3* (LV-Oit3) was transfected into macrophages, and LPS- and IFN-γ- or recombinant IL-4- and IL-13-induced polarization experiment was also performed (Fig. 6a, b). M2 macrophages possess antiinflammatory and protumorigenic features and tend to depend on oxidative phosphorylation. Similar to OIT3, the mechanistic target of rapamycin (mTOR) and adenosine 5-monophosphate-activated protein kinase (AMPK) were highly expressed in the LV-Oit3 group polarized by IL-4 and IL-13 than in the other treatment groups (Fig. 6b). We also determined the transcription levels of antiinflammatory and proinflammatory cytokines and chemokines, and key enzymes in glucose and lipid metabolism. The expression of
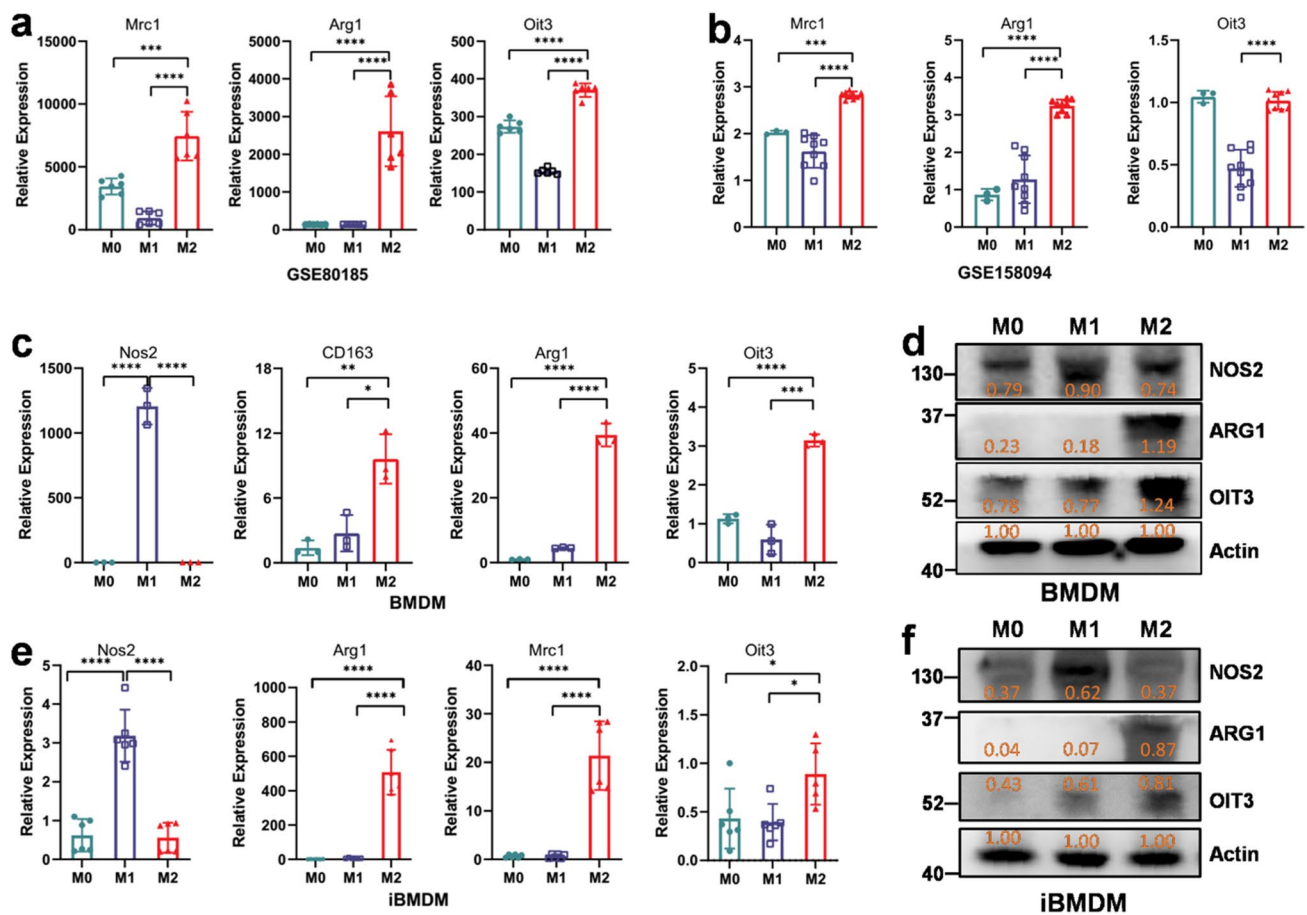
Fig. 5 OIT3 is a potential marker of M2 macrophages in GEO datasets and in vitro experiments. (**a, b**) *Mrc1*, *Arg1*, and *OIT3* expression in M0, M1, and M2 macrophages in the validate dataset of GSE80815 array data (**a**) and GSE158094 RNA-seq data (**b**). (**c–f**) Expression of M1 and M2 markers as well as OIT3 in M0, M1 and M2 BMDM (**c, d**) and iBMDM (**e, f**). Data of **a** ($n=6$), **b** ($n=3$ in M0, $n=9$ in M1 and M2), **c** ($n=3$) and **e** ($n=6$) are expressed as mean ± SEM. *$p<0.05$, **$p<0.01$, ***$p<0.001$, ****$p<0.0001$. Data of **d** and **f** are normalized against the expression of Actin

a majority of the antiinflammatory cytokines or chemokines, such as *IL10, TGFB, CCL17,* and *VEGF*, and key enzymes in fatty acid metabolism—*ACLY*, *FASN*, *CPT1A*, *LIPE*, and *GPAM*—was enhanced in M2 macrophages. In contrast, expression of proinflammatory cytokines or chemokines, including *TNF*, *IL1B*, *NOS2*, *CCL4*, *CCL5* and *CXCL2*, and enzymes *GLUT1*, *HK2*, and *PFKFB3* in glycolysis was upregulated in M1 macrophages (Fig. 6c). Thus, OIT3 may be involved in the regulation of macrophage polarization and metabolism.

Macrophage OIT3 enhances migration, invasion, and development of cancer

It is well known that M2 macrophages contribute to carcinogenesis and cancer development [11, 12, 14, 36]. We found that *OIT3*-overexpressing M2 macrophages had increased levels of MMP2 and VEGFA that promoted cancer metastasis and progression (Fig. 6c). To better understand the molecular

function of OIT3 in M2 macrophages, LV-Oit3-iBMDMs were cocultured with the HCC cell lines H22 and Hepa1-6. Interestingly, the expression of molecules related to invasion and metastasis—vimentin and Snail—was significantly increased in H22 cells cocultured with LV-Oit3-iBMDM than expression in H22 cells alone (Fig. 7a). The transwell experiment showed increased invasion and migration in the LV-Oit3-iBMDM–HCC cell coculture groups than that in negative control and mock groups (Fig. 7b, c). Moreover, the in vivo tumor volumes increased significantly in the H22 group co-injected with LV-Oit3-iBMDM than mock group and control group. Similar results were observed in tumor weights or ratios of tumor weight *versus* the body weight (Fig. 7d, e). These results demonstrate that OIT3 promotes cancer development.
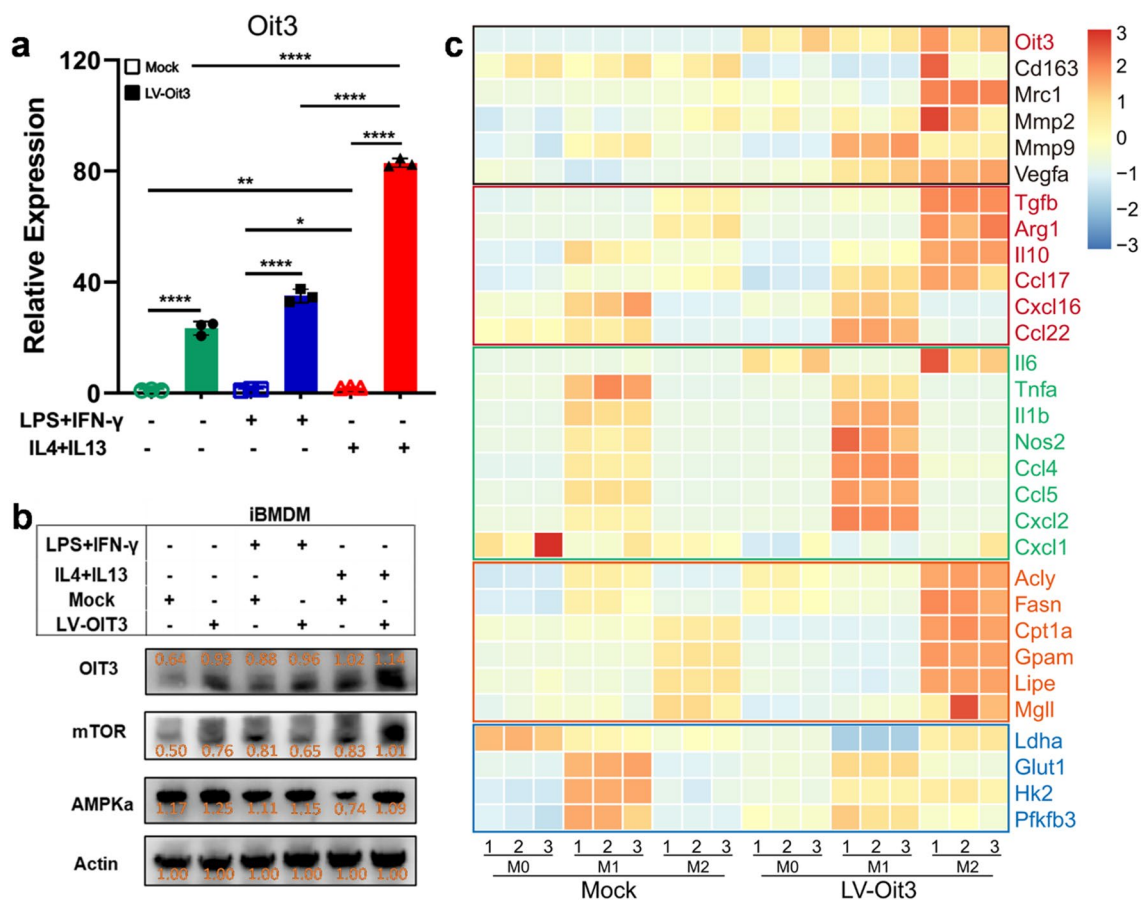
Fig. 6 OIT3 remodeled immunity and reprogrammed metabolism of macrophages. **a** Expression of OIT3 gene in iBMDM after transfected with mock or lentiviral vector of OIT3 and stimulated with PBS, LPS *plus* IFN, or IL-4 *plus* IL-13. Data are expressed as mean $\pm$ SEM ($n = 3$). $*p < 0.05$, $**p < 0.01$, $****p < 0.0001$. **b** The protein expression of OIT3, mTOR, AMPKα in iBMDM after transfected with mock or lentiviral vector of OIT3 and stimulated with PBS, LPS plus IFN, or IL-4 plus IL-13 for 48 h, respectively. The orange values indi-

cated the relative expression according to the density, the expression values were normalized against the expression of actin. **c** The transcription levels of molecules in promoting tumor (black), antiinflammatory (red), and proinflammatory (green) cytokines or chemokines, enzymes of glycolysis (blue), and fatty acid metabolism (orange) in M0, M1, and M2 macrophages after transfected with mock or lentiviral vector (LV) of OIT3

Discussion

Immunotherapy, especially PD1 or PD-L1 antibodies, has led to a paradigm shift in cancer treatment for several years. However, a majority of patients with HCC failed to benefit from immunotherapy [2, 3]. TAMs are significant components of the HCC microenvironment and are commonly associated with a poor prognosis in patients with HCC [13, 14]. Therefore, it is important to understand the pivotal roles of TAMs in the crosstalk between cytotoxic T cells and cancer cells in HCC progression, and develop novel effective treatment strategies. In this study, we found that accumulation of immune cells in paracancerous tissues correlated with tumor progression. OIT3 was validated as a novel marker of alternatively activated macrophages that play important roles in remodeling immunity and reprogramming metabolism of macrophages. Overexpression of

OIT3 in macrophages enhanced cell migration and invasion in HCC cells and promoted cancer metastasis.

Paracancer tissues, also known as peritumor, tumor-nearby, or tumor-adjacent tissues, are widely used as normal internal reference in cancer studies. However, recent studies have shown that paracancer tissues are in a preneoplastic state with molecularly altered cells and abnormal immune features [7–10]. The data from our previous study validated that the infiltrated immune cells tended to accumulate in paracancer tissues [9] that are frequent sites for cancer progression and metastasis. The present study indicated that M2 macrophages of paracancer tissues facilitate cancer cell migration and invasion, and highlighted the indispensable role of paracancer tissue in the TME.

OIT3 is a liver-specific, zona pellucida domain-containing protein (LZP) that is primarily expressed in hepatocytes and rarely in other organs [37]. However,
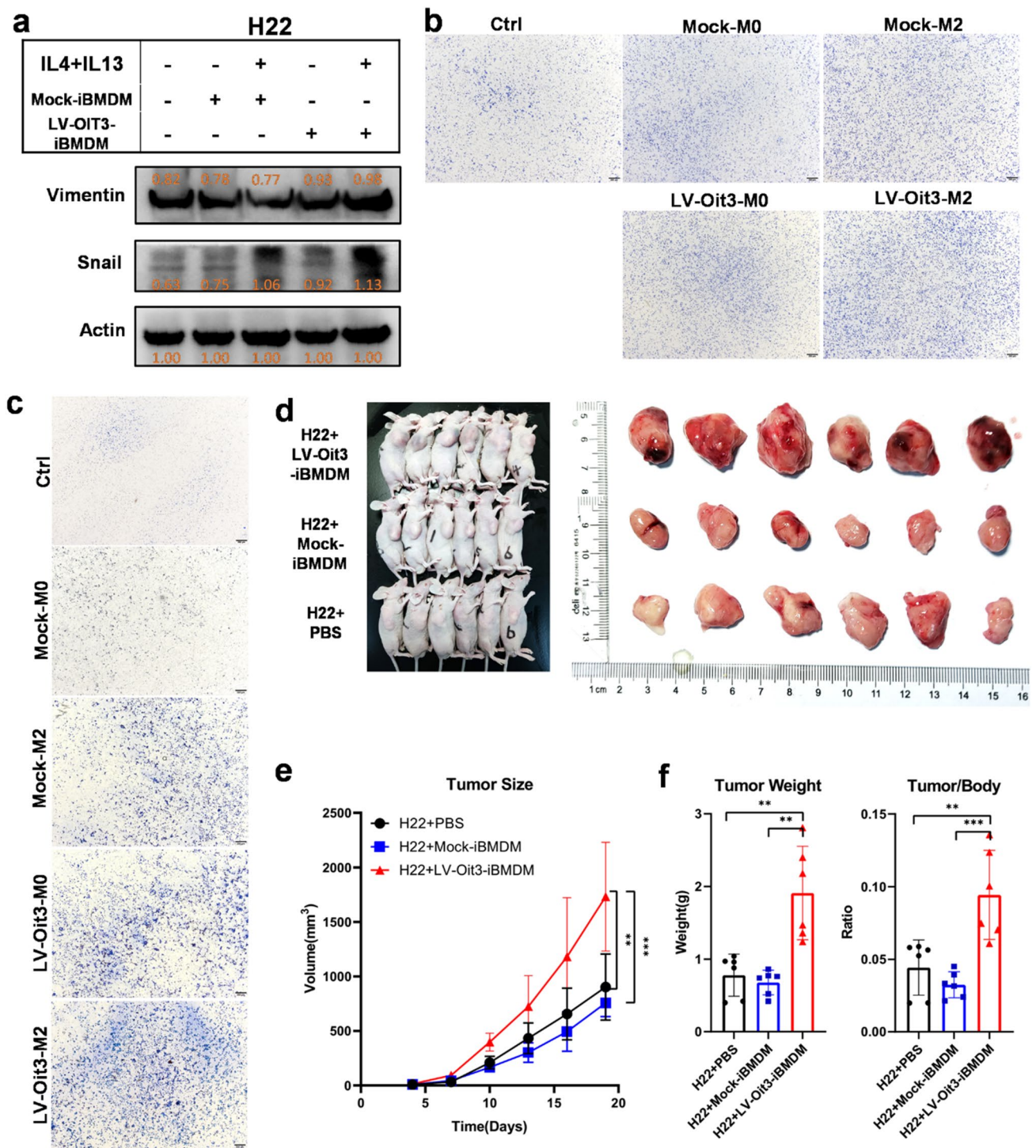
Fig. 7 Macrophage OIT3 enhanced migration, invasion, and development of cancer. **a** The protein expression of Vimentin and Snail in H22 cells cocultured with Mock-iBMDMs or LV-Oit3-iBMDM with or without M2 polarized by IL4 and IL13. The orange values indicated the relative expression according to the density; the expression values were normalized against the expression of Actin. **b** Hepa1-6 cells were cocultured with Mock-iBMDMs or LV-Oit3-iBMDMs with or without M2 polarized by IL4 plus IL13 for 12 h. The ratios of immigrated cells versus area were 42.23, 52.25, 52.57, 62.39, and 62.75, respectively. **c** Hepa1-6 cells were cocultured with Mock-iBMDMs or LV-Oit3-iBMDMs with or without polarized by IL4 and IL13 for 24 h. The ratios of invasive cells versus area were 38.09, 69.93, 82.40, 85.56, and 108.75, respectively. **d–f** Mice were injected *i.h.* with H22+PBS, H22+Mock-iBMDM and H22+LV-Oit3-iBMDM, respectively. Tumor entity view from groups (**d**), curves of tumor volume (**e**), tumor weight (left) and tumor/body ratio (right) (**f**). Data of **e** and **f** were are expressed as mean±SEM ($n=6$). ** $p < 0.01$, *** $p < 0.001$

the expression of OIT3 significantly decreases in HCC. Interestingly, a study indicated that OIT3 had no significant effect on cancer cell proliferation in vitro and tumor growth in vivo [38]. Moreover, recent studies revealed that OIT3 maintains urate homeostasis in the renal tubules and is required for hepatic triacylglycerol transportation [39, 40]. In the present study, we identified OIT3 as a novel biomarker of M2 macrophages that performed as reliably as MRC1 and ARG1.

The metabolic profile of macrophages is closely associated with cancer progression and anticancer immunotherapy. mTOR, a serine/threonine kinase, mediates M1 polarization by reducing the secretion of antiinflammatory cytokines and increasing secretion of proinflammatory cytokines [41], whereas AMPK, a key factor in oxidative phosphorylation, suppresses M1 polarization by attenuating glycolysis [42]. In the present study, the expression of AMPK and mTOR both increased in macrophages overexpressing OIT3, indicating a relative paradox in reprogramming metabolism. The expression of key enzymes in lipid metabolism increased, whereas that of key enzymes in glycolysis decreased. Moreover, a majority of antiinflammatory cytokines and chemokines were highly expressed in M2 macrophages overexpressing *OIT3*. Additionally, these *OIT3*-overexpressing macrophages enhanced the migration and invasion of cancer cells and promoted tumorigenesis and progression.

In conclusion, the study identified OIT3 as a novel biomarker of M2 macrophages in paracancer tissues that remodeled immune features and reprogrammed metabolism in macrophages. Targeting OIT3 in macrophages may impede cancer cell migration and invasion and dampen tumorigenesis and cancer development.

Declarations

Conflict of interest The authors declare no competing interests.

Consent to participate Informed consent was obtained from all individual participants included in the study.

Ethics approval This study was performed in line with the principles of the Declaration of Helsinki. Approvals were obtained by the Institutional Review Board of the Army Medical University and Chongqing University.

References

1. Sung H, Ferlay J, Siegel RL, Laversanne M, Soerjomataram I, Jemal A et al (2021) Global cancer statistics 2020: globocan estimates of incidence and mortality worldwide for 36 cancers in 185 countries. CA Cancer J Clin 71:209–249. https://doi.org/10.3322/caac.21660
2. Yang JD, Heimbach JK (2020) New advances in the diagnosis and management of hepatocellular carcinoma. BMJ 371:m3544. https://doi.org/10.1136/bmj.m3544
3. Llovet JM, Montal R, Sia D, Finn RS (2018) Molecular therapies and precision medicine for hepatocellular carcinoma. Nat Rev Clin Oncol 15:599–616. https://doi.org/10.1038/s41571-018-0073-4
4. Galon J, Bruni D (2020) Tumor immunology and tumor evolution: Intertwined histories. Immunity 52:55–81. https://doi.org/10.1016/j.immuni.2019.12.018
5. Zhu AX, Finn RS, Edeline J, Cattan S, Ogasawara S, Palmer D et al (2018) Pembrolizumab in patients with advanced hepatocellular carcinoma previously treated with sorafenib (keynote-224): a non-randomised, open-label phase 2 trial. Lancet Oncol 19:940–952. https://doi.org/10.1016/s1470-2045(18)30351-6
6. El-Khoueiry AB, Sangro B, Yau T, Crocenzi TS, Kudo M, Hsu C et al (2017) Nivolumab in patients with advanced hepatocellular carcinoma (checkmate 040): an open-label, non-comparative, phase 1/2 dose escalation and expansion trial. Lancet (London, England) 389:2492–2502. https://doi.org/10.1016/s0140-6736(17)31046-2
7. Hoshida Y, Villanueva A, Kobayashi M, Peix J, Chiang DY, Camargo A et al (2008) Gene expression in fixed tissues and outcome in hepatocellular carcinoma. N Engl J Med 359:1995–2004. https://doi.org/10.1056/NEJMoa0804525
8. Aran D, Camarda R, Odegaard J, Paik H, Oskotsky B, Krings G et al (2017) Comprehensive analysis of normal adjacent to tumor transcriptomes. Nat Commun 8:1077. https://doi.org/10.1038/s41467-017-01027-z
9. Yeung OW, Lo CM, Ling CC, Qi X, Geng W, Li CX et al (2015) Alternatively activated (m2) macrophages promote tumour growth and invasiveness in hepatocellular carcinoma. J Hepatol 62:607–616. https://doi.org/10.1016/j.jhep.2014.10.029
10. Graham K, Ge X, de Las MA, Tripathi A, Rosenberg CL (2011) Gene expression profiles of estrogen receptor–positive and estrogen receptor–negative breast cancers are detectable in histologically normal breast epithelium. Clin Cancer Res 17:236–246. https://doi.org/10.1158/1078-0432.CCR-10-1369
11. Krenkel O, Tacke F (2017) Liver macrophages in tissue homeostasis and disease. Nat Rev Immunol 17:306–321. https://doi.org/10.1038/nri.2017.11
12. Komohara Y, Fujiwara Y, Ohnishi K, Takeya M (2016) Tumor-associated macrophages: potential therapeutic targets for anticancer therapy. Adv Drug Deliv Rev 99:180–185. https://doi.org/10.1016/j.addr.2015.11.009

13. Gok Yavuz B, Hasanov E, Lee SS, Mohamed YI, Curran MA, Koay EJ et al (2021) Current landscape and future directions of biomarkers for immunotherapy in hepatocellular carcinoma. J Hepatocell Carcinoma 8:1195–1207. https://doi.org/10.2147/jhc.S322289

14. Mantovani A, Allavena P (2015) The interaction of anticancer therapies with tumor-associated macrophages. J Exp Med 212:435–445. https://doi.org/10.1084/jem.20150295

15. Zhao H, Yan G, Zheng L, Zhou Y, Sheng H, Wu L et al (2020) Stim1 is a metabolic checkpoint regulating the invasion and metastasis of hepatocellular carcinoma. Theranostics 10:6483–6499. https://doi.org/10.7150/thno.44025

16. Zhang B, Horvath S (2005) A general framework for weighted gene co-expression network analysis. Stat Appl Genet Mol Biol. https://doi.org/10.2202/1544-6115.1128

17. Langfelder P, Horvath S (2008) Wgcna: an r package for weighted correlation network analysis. BMC Bioinform 9:559. https://doi.org/10.1186/1471-2105-9-559

18. Zhang X, Wu L, Xu Y, Yu H, Chen Y, Zhao H et al (2020) Microbiota-derived ssl6 enhances the sensitivity of hepatocellular carcinoma to sorafenib by down-regulating glycolysis. Cancer Lett 481:32–44. https://doi.org/10.1016/j.canlet.2020.03.027

19. Li Y, Guo B, Xie Q, Ye D, Zhang D, Zhu Y et al (2015) Stim1 mediates hypoxia-driven hepatocarcinogenesis via interaction with hif-1. Cell Rep 12:388–395. https://doi.org/10.1016/j.celrep.2015.06.033

20. Wickham H (2016) Ggplot2: elegant graphics for data analysis. Springer-Verlag, New York

21. Yang Z, Li Q, Wang X, Jiang X, Zhao D, Lin X et al (2018) C-type lectin receptor lsectin-mediated apoptotic cell clearance by macrophages directs intestinal repair in experimental colitis. Proc Natl Acad Sci USA 115:11054–11059. https://doi.org/10.1073/pnas.1804094115

22. Bénézech C, Nayar S, Finney BA, Withers DR, Lowe K, Desanti GE et al (2014) Clec-2 is required for development and maintenance of lymph nodes. Blood 123:3200–3207. https://doi.org/10.1182/blood-2013-03-489286

23. Rydz N, Swystun LL, Notley C, Paterson AD, Riches JJ, Sponagle K et al (2013) The c-type lectin receptor clec4m binds, internalizes, and clears von willebrand factor and contributes to the variation in plasma von willebrand factor levels. Blood 121:5228–5237. https://doi.org/10.1182/blood-2012-10-457507

24. Cereijo R, Gavaldà-Navarro A, Cairó M, Quesada-López T, Villarroya J, Morón-Ros S et al (2018) Cxcl14, a brown adipokine that mediates brown-fat-to-macrophage communication in thermogenic adaptation. Cell Metab 28:750–63.e6. https://doi.org/10.1016/j.cmet.2018.07.015

25. Tang B, Zhu J, Zhao Z, Lu C, Liu S, Fang S et al (2021) Diagnosis and prognosis models for hepatocellular carcinoma patient's management based on tumor mutation burden. J Adv Res 33:153–165. https://doi.org/10.1016/j.jare.2021.01.018

26. Thorsson V, Gibbs DL, Brown SD, Wolf D, Bortone DS, Ou Yang TH et al (2018) The immune landscape of cancer. Immunity 48(812–30):e14. https://doi.org/10.1016/j.immuni.2018.03.023

27. Newman AM, Steen CB, Liu CL, Gentles AJ, Chaudhuri AA, Scherer F et al (2019) Determining cell type abundance and expression from bulk tissues with digital cytometry. Nat Biotechnol 37:773–782. https://doi.org/10.1038/s41587-019-0114-2

28. Newman AM, Liu CL, Green MR, Gentles AJ, Feng W, Xu Y et al (2015) Robust enumeration of cell subsets from tissue expression profiles. Nat Methods 12:453–457. https://doi.org/10.1038/nmeth.3337

29. Chen B, Khodadoust MS, Liu CL, Newman AM, Alizadeh AA (2018) Profiling tumor infiltrating immune cells with cibersort.

30. Zuccolo J, Deng L, Unruh TL, Sanyal R, Bau JA, Storek J et al (2013) Expression of ms4a and tmem176 genes in human b lymphocytes. Front Immunol 4:195. https://doi.org/10.3389/fimmu.2013.00195

31. Fischer-Riepe L, Daber N, Schulte-Schrepping J, Véras De Carvalho BC, Russo A, Pohlen M et al (2020) Cd163 expression defines specific, irf8-dependent, immune-modulatory macrophages in the bone marrow. J Allergy Clin Immunol 146:1137–1151. https://doi.org/10.1016/j.jaci.2020.02.034

32. Liu D, Lu Q, Wang X, Wang J, Lu N, Jiang Z et al (2019) Lsectin on tumor-associated macrophages enhances breast cancer stemness via interaction with its receptor btn3a3. Cell Res 29:365–378. https://doi.org/10.1038/s41422-019-0155-6

33. Kim KH, Choi BK, Kim YH, Han C, Oh HS, Lee DG et al (2016) Extracellular stimulation of vsig4/complement receptor ig suppresses intracellular bacterial infection by inducing autophagy. Autophagy 12:1647–1659. https://doi.org/10.1080/15548627.2016.1196314

34. Chakarov S, Lim HY, Tan L, Lim SY, See P, Lum J et al (2019) Two distinct interstitial macrophage populations coexist across tissues in specific subtissular niches. Science (New York, NY). https://doi.org/10.1126/science.aau0964

35. Lim HY, Lim SY, Tan CK, Thiam CH, Goh CC, Carbajo D et al (2018) Hyaluronan receptor lyve-1-expressing macrophages maintain arterial tone through hyaluronan-mediated regulation of smooth muscle cell collagen. Immunity 49:326–41.e7. https://doi.org/10.1016/j.immuni.2018.06.008

36. Lee YH, Tai D, Yip C, Choo SP, Chew V (2020) Combinational immunotherapy for hepatocellular carcinoma: radiotherapy, immune checkpoint blockade and beyond. Front Immunol 11:568759. https://doi.org/10.3389/fimmu.2020.568759

37. Xu ZG, Du JJ, Cui SJ, Wang ZQ, Huo KK, Li YY et al (2004) Identification of lzp gene from mus musculus and rattus norvegicus coding for a novel liver-specific zp domain-containing secretory protein. DNA Seq J DNA Seq Mapp 15:81–87. https://doi.org/10.1080/10425170310001652200

38. Xu ZG, Du JJ, Zhang X, Cheng ZH, Ma ZZ, Xiao HS et al (2003) A novel liver-specific zona pellucida domain containing protein that is expressed rarely in hepatocellular carcinoma. Hepatology 38:735–744. https://doi.org/10.1053/jhep.2003.50340

39. Wu JX, He KY, Zhang ZZ, Qu YL, Su XB, Shi Y et al (2021) Lzp is required for hepatic triacylglycerol transportation through maintaining apolipoprotein b stability. PLoS Genet 17:e1009357. https://doi.org/10.1371/journal.pgen.1009357

40. Yan B, Zhang ZZ, Huang LY, Shen HL, Han ZG (2012) Oit3 deficiency impairs uric acid reabsorption in renal tubule. FEBS Lett 586:760–765. https://doi.org/10.1016/j.febslet.2012.01.038

41. Byles V, Covarrubias AJ, Ben-Sahra I, Lamming DW, Sabatini DM, Manning BD et al (2013) The tsc-mtor pathway regulates macrophage polarization. Nat Commun 4:2834. https://doi.org/10.1038/ncomms3834

42. Wang S, Liu R, Yu Q, Dong L, Bi Y, Liu G (2019) Metabolic reprogramming of macrophages during infections and cancer. Cancer Lett 452:14–22. https://doi.org/10.1016/j.canlet.2019.03.015

Methods Mol Biol 1711:243–259. https://doi.org/10.1007/978-1-4939-7493-1_12

Publisher's Note Springer Nature remains neutral with regard to jurisdictional claims in published maps and institutional affiliations.